Biosensors and Bioelectronics 86 (2016) 958–965

Contents lists available at ScienceDirect

Biosensors and Bioelectronics

journal homepage: www.elsevier.com/locate/bios

Hemin on graphene nanosheets functionalized with flower-like MnO_2 and hollow AuPd for the electrochemical sensing lead ion based on the specific DNAzyme

Shuyan Xue, Pei Jing, Wenju Xu *

Key Laboratory of Luminescent and Real-Time Analytical Chemistry (Southwest University), Ministry of Education, School of Chemistry and Chemical Engineering, Southwest University, Chongqing 400715, PR China

ARTICLE INFO

Article history:
Received 3 July 2016
Received in revised form
28 July 2016
Accepted 29 July 2016
Available online 30 July 2016

Keywords:
Electrochemical sensor
Lead ion
Flower-like MnO_2
Hollow AuPd
Pb^{2+}-specific DNAzyme

ABSTRACT

Herein, integrated with DNAzyme highly specific to metal ions, hemin@reduced graphene oxide (hemin@rGO) functionalized with flower-like MnO_2 and hollow AuPd (hAuPd-fMnO_2-hemin@rGO) was used as electroactive probe and electrocatalyst to construct a universal platform for metal ion detection (lead ion Pb^{2+} as the model). The proposed strategy with generality was mainly based on two aspects. Firstly, the designed probe not only showed high stability and excellent peroxidase-like activity originating from hemin, fMnO_2 and hAuPd, but also possessed intrinsic redox performance from hemin, which resulted in the promotion of electron transfer and the enhancement of the response signal readout. Secondly, due to the introduction of Pb^{2+}, Pb^{2+}-dependent DNAzyme bound in the electrode surface could be specifically identified and cleaved by Pb^{2+}, and the remained fragment (its supplementary sequence is a single-strand DNA S3) captured the nanocomposites S3-hAuPd-fMnO_2-hemin@rGO by the hybridization reaction. Therefore, combined the cooperative catalysis of fMnO_2, hAuPd and hemin to H_2O_2 reduction with highly specific interaction of Pb^{2+}-dependent DNAzyme, the proposed Pb^{2+} biosensor showed significant improvement of electrochemical analytical performance, which was involved in wide dynamic response in the range of 0.1 pM–200 nM, low detection limit of 0.034 pM, high sensitivity and high specificity. This could facilitate the universal strategy to be a promising method for detection of other metal ions, only changing the corresponding DNAzyme specific to them.

1. Introduction

Owing to the difficult biodegradation and easy accumulation in soft tissues, metal ions, especially heavy metal ions, such as mercury ions (Hg^{2+}), copper ions (Cu^{2+}) and lead ions (Pb^{2+}) have been considered as the serious source of environment pollution and many healthy diseases of living beings (Cui et al., 2015a, 2015b, 2015c; Kim et al., 2015). Therefore, sensitive and selective assay of heavy metal ions is of considerable significance. DNAzyme is a kind of in vitro selected DNA molecules with enzymatic catalytic activities (B. Zhang et al., 2015; J. Zhang et al., 2015). Among them, DNAzyme with metal ion-dependent activity have attracted intensive attention because of the simple synthesis, good stability, and especially high metal ion specificity (Y. Zhang et al., 2013; Z.X. Zhang et al., 2013). As a result, many DNAzyme-based sensors have been developed for the determination of metal ions. Cui et al. (2015b, 2015c) reported an electrochemical Pb^{2+} sensor using a DNA functionalized porphyrinic metal-organic framework, and other research group used L-DNAzyme to design a novel fluorescence sensing platform to Cu^{2+} and Pb^{2+} (Cui et al., 2015a). Among these analytical methods, the electrochemical strategies are more attractive due to many desirable advantages including simple operation, exceptional portability, high sensitivity and long stability (Liu et al., 2012; Xiao et al., 2007).

In order to further improve the sensitivity of the detection method, numerous enzymes such as horseradish peroxidase and glucose oxidase have been commonly used for signal amplification of the electrochemical sensors (Wan et al., 2015; H.W. Wang et al., 2013; M.H. Wang et al., 2013). However, the practical applications of such enzyme-based strategies are limited by complicated immobilization procedures, insufficient long-term stability and high cost (Ju et al., 2015). Thus, various nanomaterials with electrocatalytic activity have been introduced as alternatives of enzymes to construct sensitive electrochemical sensors (Jiang et al., 2016; Zhou et al., 2015; Wan et al., 2015). Although these works could achieve trace detection of Pb^{2+}. More significant enhancement of response signal and improvement of sensitivity are still urgently needed in the field of analytical chemistry. Recently, flower-like

* Corresponding author.
E-mail address: xwju@swu.edu.cn (W. Xu).

http://dx.doi.org/10.1016/j.bios.2016.07.111
0956-5663/

manganese oxide ($fMnO_2$) nanospheres (NSs) have received intensive research interest, owing to the low cost, large surface area, especially high peroxidase-like activity and good chemical stability (Kuo et al., 2014; Zhang et al., 2014; Y. Zhang et al., 2013; Z.X. Zhang et al., 2013). Nevertheless, the electrochemical performance of $fMnO_2$ NSs is limited by poor electrical conductivity (Hou et al., 2010). To face the challenge, hollow AuPd (hAuPd) nanoparticles (NPs) with the good electrical conductivity and catalytic activity are integrated with $fMnO_2$ NSs (Chang et al., 2015; Chai et al., 2011; Darabdhara et al., 2015). Moreover, hAuPd NPs are of large surface area beyond the solid counterparts (Shang et al., 2015), which potentially makes them be excellent candidates for catalysis and sensing. Therefore, the combination of $fMnO_2$ NSs and hAuPd NPs would be extremely attractive for fabricating highly sensitive electrochemical sensors.

Herein, combined with the highly specific interaction of metal ion-dependent DNAzyme, hemin at reduced graphene oxide (hemin@rGO) functionalized with flower-like MnO_2 and hollow AuPd (hAuPd-$fMnO_2$-hemin@rGO) was used to construct an universal electrochemical platform sensing metal ions, such as Pb^{2+}, a major and persistent environmental pollutant which is capable of causing serious diseases (Zang et al., 2014). In the presence of Pb^{2+}, Pb^{2+}-dependent DNAzyme was specifically identified and cleaved by Pb^{2+}, and the remained fragment in the electrode substrate captured the bioconjugates of hAuPd-$fMnO_2$-hemin@rGO immobilized with a single-strand DNA by hybridization reaction. Under the synergetic catalysis of $fMnO_2$, hAuPd and hemin, the great promotion of electron transfer in the electrode surface and the significant enhancement of electrochemical response was successfully achieved. This could enable the proposed strategy for Pb^{2+} detection to have outstanding improvement in analytical performance, such as wide linear range, low detection limit, high specificity and relative low cost (Li et al., 2012), which may be potentially promising to establish such sensing system for monitoring other metal ions, only changing the corresponding specific DNAzyme.

2. Experimental

2.1. Reagents and materials

Lead nitrate ($Pb(NO_3)_2 \cdot 3H_2O$), hemin, gold chloride ($HAuCl_4 \cdot 4H_2O$), potassium tetrachloropalladate (K_2PdCl_4), bovine serum albumin (BSA, 96–99%), N-(3-dimethylaminopropyl)-N′-ethylcarbodiimidehydrochloride (EDC), N-hydroxy succinimide (NHS) and poly(ethylenimine) (PEI) were purchased from Sigma-Aldrich Chemical Co. (St. Louis, MO, USA). 3-Aminopropyltriethoxysilane (APTES, 98%) was obtained from Beijing Bailingwei Chemical Technology Co., Ltd. (Beijing, China). Potassium permanganate ($KMnO_4$), trisodium citrate dihydrate ($C_6H_5Na_3O_7 \cdot 2H_2O$), ascorbic acid (AA) and cobalt chloride ($CoCl_2 \cdot 6H_2O$) were received from Chengdu Kelong Chemical Reagent Company (Chengdu, China). Hydrazine hydrate ($N_2H_4 \cdot H_2O$), glutaraldehyde (GA) and oleic acid were purchased from Beijing Chemical Reagent Co. (Beijing, China). Graphene oxide (GO) was obtained from Nanjing Xianfeng Nano Go. (Nanjing, China). Trishydroxymethylaminomethane hydrochloride (Tris-HCl) was purchased from Roche (Switzerland). The substrate strand and catalytic strand of Pb^{2+}-dependent DNAzyme were supplied by Sangon Biotech. Inc. (Shanghai, China). The sequences of the corresponding oligonucleotides were listed as follows: substrate strand (S1): 3′-SH-$(CH_2)_6$-GTAGAGAAGG rA TATCACTCA-5′ (rA-cleavage site), catalytic strand (S2): 5′-CATCTCTTCTCC-GAGCCGGTCGAAATAGTGAGT-3′, and complementary DNA strand (S3): 5′-CATCTCTTCC-$(CH_2)_6$-SH-3′, which is complementary to the sequence of S1 from 3′ terminal to rA. Double-distilled water (DD water) obtained from a Milliporewater purification system ($\geq$ 18.2 MΩ, Milli-Q, Millipore) was used throughout the experiment. All other reagents were of analytical grade and used as received.

2.2. Apparatus

Differential pulse voltammetry (DPV) and cyclic voltammetry (CV) were conducted using a CHI 660C electrochemical workstation (Shanghai Chenhua Instrument, China) in a conventional three electrode system. A bare or modified glassy carbon electrode (GCE, 4 mm in diameter) was used as the working electrode with a saturated calomel electrode (SCE) as the reference electrode and a platinum wire as the auxiliary electrode. Electrochemical impedance spectroscopy (EIS) was performed using a CHI 660D electrochemical workstation (Shanghai Chenhua Instrument, China). The scanning electron micrographs was taken using a scanning electron microscope (SEM, S-4800, Hitachi Instrument, Japan). X-ray photoelectron spectroscopy (XPS) was conducted using the Thermo ESCALAB 250Xi spectrometer with Al Ka X-ray (1486.6 eV) as the light source (Thermoelectricity Instruments, USA). UV–vis absorption spectra were recorded using a UV-2450 UV–vis spectrophotometer in the range of 200–800 nm (Shimadzu, Japan). Resonance Raman spectra were recorded on a LabRAM HR 800 Raman spectrophotometer (Jobin Yvon, France). pH measurement was conducted with a pH meter (MP 230, Mettler-Toledo, Switzerland).

2.3. Preparation of hemin functionalized reduced graphene oxide (hemin@rGO)

Hemin@rGO was prepared according to the published method in the literature (Li et al., 2016). Briefly, 10 mL of homogeneous GO dispersion (0.5 mg/mL) in H_2O was mixed with 10 mL of hemin solution (0.5 mg/mL) in H_2O, 100 μL of ammonia solution (25%) and 15 μL hydrazine solution. After vigorous stirring for about 0.5 h, the mixture was allowed in a water bath for 3.5 h at 60 °C. Finally, hemin was attached onto rGO surface through π-π stacking (Luo et al., 2013). The obtained hemin@rGO was centrifugated out, washed with DD water for several times, and re-dispersed in 5 mL of DD water for further use.

2.4. Preparation of flower-Like MnO_2 nanospheres functionalized with APTES (APTES-$fMnO_2$)

Based on the previous literature with little modification (Y. Zhang et al., 2013; Z.X. Zhang et al., 2013), APTES-$fMnO_2$ nanospheres (NSs) were obtained by functionalizing $fMnO_2$ NSs with APTES, which resulted in the numerous NH_2 groups presented in $fMnO_2$ NSs surface. In a typical procedure, $KMnO_4$ (0.5 g) was suspended in 250 mL H_2O under magnetically stirring for about 0.5 h, followed by the addition of oleic acid (5 mL) and magnetically string for another 0.5 h. The obtained precipitate was centrifuged, washed with DD water and alcohol for several times and redispersed in 3 mL water. The obtained $fMnO_2$ NSs was dried under vacuum at 60 °C. Then, a mixture of the as-synthesized $fMnO_2$ NSs (0.25 g), toluene (80 mL) and APTES (0.5 mL) was stirred and refluxed at 120 °C under N_2 for 6 h. After that, the APTES-$fMnO_2$ with –NH_2 group was obtained by centrifugation, and washing with toluene and distilled water for several times, and was re-dispersed in 12 mL of PBS (0.1 M, pH 7.4) for the subsequent use.

2.5. Preparation of hollow AuPd nanoparticles (hAuPd NPs)

The hAuPd NPs were prepared by using the previous method with minor modification (Shang et al., 2015). Briefly, 4.25 mg $CoCl_2 \cdot 6H_2O$ and 10 mg $C_6H_5Na_3O_7 \cdot 2H_2O$ were dispersed in 25 mL H_2O, followed by stirring for 30 min under N_2 at room temperature. Next, 10 mL of freshly prepared $NaBH_4$ (1 mg/mL) was added into the above mixture with keeping 30 min stirring under N_2. The change of the resultant solution from colorless to brown-black suggested the successful formation of Co NPs. Then, $HAuCl_4 \cdot 4H_2O$ (100 μL, 20 mM) and K_2PdCl_4 (800 μL, 10 mM) were simultaneously added slowly into the above mixture. After stirring for another 15 min under N_2, Co NPs as templates were fully oxidized by $HAuCl_4$ and Na_2PdCl_4 to Co (II). Finally, the product hAuPd NPs were obtained by centrifugation and washing with DD water and re-dispersed in 5 mL H_2O.

Similarly, hollow Au (hAu) NPs were synthesized by varying the molar ratio of $HAuCl_4$ and K_2PdCl_4 as 1:0. And solid AuPd (sAuPd) NPs were prepared by replacing 10 mL $NaBH_4$ into 1 mL ascorbic acid (0.1 M) in the absence of Co NPs as templates.

2.6. Preparation of hemin@rGO conjugated with $fMnO_2$, hAuPd and S3 (S3-hAuPd-$fMnO_2$-hemin@rGO)

1 mg NHS and 4 mg EDC were added into 1 mL of the as-prepared hemin@rGO with the subsequent addition of 300 μL APTES-$fMnO_2$ under stirring at room temperature, followed by the introduction of 300 μL hAuPd NPs. After stirring for 12 h, the nanocomposites of hAuPd-$fMnO_2$-hemin@rGO were prepared through the strong interaction of Au-N bond and/or Pd-N bond. Next, the obtained precipitate was centrifugated and resuspended in 0.5 mL H_2O, in which 200 μL of 2.5 μM complementary DNA (S3) was injected and stirred overnight under 4 °C. After that, S3 was attached to hAuPd NPs surface through Au–S bond or Pd–S bond, resulting in the formation of the bioconjugates of S3-hAuPd-$fMnO_2$-hemin@rGO. The final introduction of 50 μL of BSA (*w*/*w*, 1%) was to block the remaining active sites for stirring 40 min at 4 °C to obtain the proposed product through centrifugation and resuspending in 1 mL of H_2O.

Herein, in order to specifically demonstrate the utility of the proposed bioconjuates of S3-hAuPd-$fMnO_2$-hemin@rGO, other three bioconjuates of S3 with hAuPd-hemin@rGO, hAu-$fMnO_2$-hemin@rGO and sAuPd-$fMnO_2$-hemin@rGO were respectively prepared according to the above method with a little modification (see supporting information for details).

2.7. Fabrication of the proposed electrochemical sensor

As shown in Scheme 1, the proposed Pb^{2+} sensor was fabricated mainly followed three steps. Firstly, a clean glassy carbon electrode (GCE) (Φ=4 mm) pretreated by polishing with 0.3 μm and 0.05 μm Al_2O_3 powder, sonicating and rinsing with DD water was electrodeposited in $HAuCl_4$ solution at constant potential of −0.2 V for 30 s to obtain depAu. Then 10 μL S1 (2.5 μM) of the substrate strand S1 terminated with –SH was modified onto the resulting electrode surface for 12 h, leading to the immobilization of S1 through Au-S affinity, followed by the incubation of 10 μL S2 (2.5 μM) for another 12 h to bind S1 for forming the Pb^{2+}-dependent DNAzyme (Note: the concentration of S1 and S2 was optimized). Secondly, after the introduction of 10 μL BSA (*w*/*w*, 1%) for 40 min, 10 μL of Pb^{2+} standard solutions with different concentrations was pipetted onto the electrode surface for 60 min to

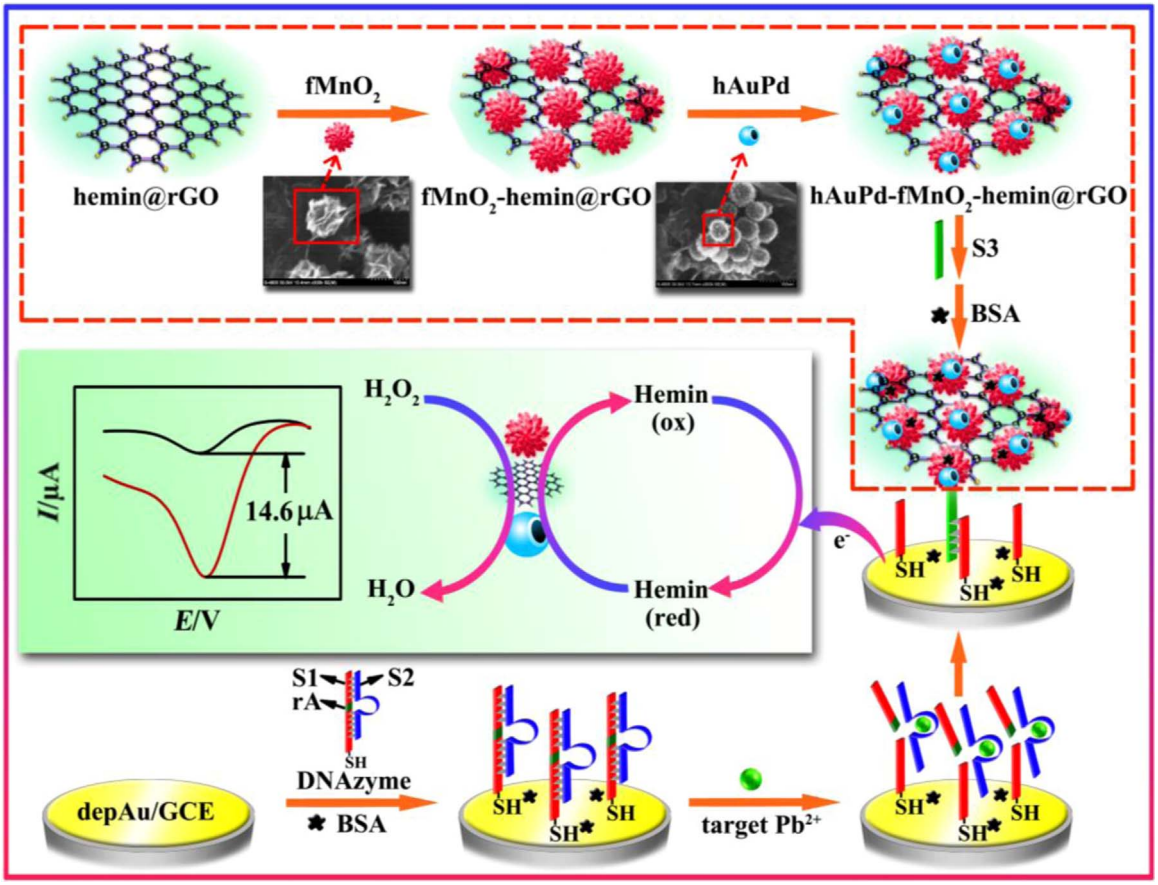

Scheme 1. Schematic diagram of the fabrication of the electrochemical sensor for Pb^{2+} detection and the signal amplification strategy.

identify and cleave the formed DNAzyme at the cleavage site rA (Note: the incubation time of Pb^{2+} was optimized). One fragment of S1 was removed from the electrode surface by washing and the other one with –SH terminal kept staying. Finally, through the hybridization reaction of S3 and the stayed one fragment, 10 μL of S3-hAuPd-fMnO_2-hemin@rGO was captured for 40 min to obtain the proposed sensor, which was washed by DD water after every modification in the electrode surface. Thus, the electrochemical signal given by hemin as the redox probe was used to sense Pb^{2+} with different concentrations.

2.8. Electrochemical measurement

20 mM Tris-HCl buffer (pH 7.0) containing 140 mM NaCl, 1 mM $CaCl_2$, 1 mM $MgCl_2$ and 5 mM KCl was used to prepare the solution of S1, S2 and S3. Phosphate buffered solution (PBS) (pH 7.0) containing 0.1 M Na_2HPO_4, 0.1 M KH_2PO_4 and 0.1 M KCl was employed as working buffer. For the proposed Pb^{2+} sensor, the modification process was characterized by measuring CV response from -0.2 to 0.6 V at 100 mV/s scan rate and EIS response with the potential of 220 mV, 5 mV amplitude and 1.0×10^{-2} Hz–1.0×10^{6} Hz frequency in 0.1 M PBS (pH 7.4) containing 5 mM $[Fe(CN)_6]^{3-/4-}$ solution. The DPV signal was measured in the potential range of -0.1 V to 0.6 V (vs. SCE) with the increment of 4 mV, pulse width of 50 s, amplitude of 50 mV and sample width of 0.0167 s in the absence or presence of 1.7 mM H_2O_2, which was used to evaluate the electrochemical performance of the proposed sensor under the optimum experimental conditions. The actual applicability of the sensor was investigated by detecting Pb^{2+} in tap water and lake water obtained from local lake, which was pretreated by centrifugation before use.

3. Results and discussion

3.1. Characterization of the nanocomposites of hAuPd-fMnO_2-hemin@rGO

Firstly, different nanocomposites including hemin@rGO, fMnO_2-hemin@rGO and hAuPd-fMnO_2-hemin@rGO were characterized by recording scanning electron microscope (SEM). As shown in Fig. 1, a typical flake-like shape of hemin@rGO was observed in Fig. 1(A), and large amounts of fMnO_2 NSs with a distinct flower-like structure were loaded onto the surface of hemin@rGO, indicating the formation of fMnO_2-hemin@rGO (Fig. 1(B)). Also from Fig. 1(C), we could see hAuPd NPs with distinct hollow structures on the surface of fMnO_2 NSs, indicating the successful preparation of hAuPd-fMnO_2-hemin@rGO.

Moreover, X-ray photoelectron spectroscopy (XPS), UV–vis absorption spectra and Raman spectra of different nanocomposites were also conducted and the results are shown in Fig. S1 and Fig. S2, respectively. All the observations were in good accordance with those reported in references.

3.2. Electrochemical behaviors of modified sensor

To characterize the fabrication process of the proposed electrochemical Pb^{2+} sensor, CV response was measured in 5 mM $[Fe(CN)_6]^{3-/4-}$ solution (pH 7.4) and the results were shown in Fig. 2 (A). Obviously, the bare GCE exhibited a typical pair of well-defined redox peaks (curve a). After the introduction of depAu in GCE surface, the peak current of the electrode depAu/GCE greatly increased (curve b), owing to the promotion of AuNPs to electron transfer. When thiol-terminated S1 and S2 were successively immobilized onto depAu/GCE surface through Au–S bond and

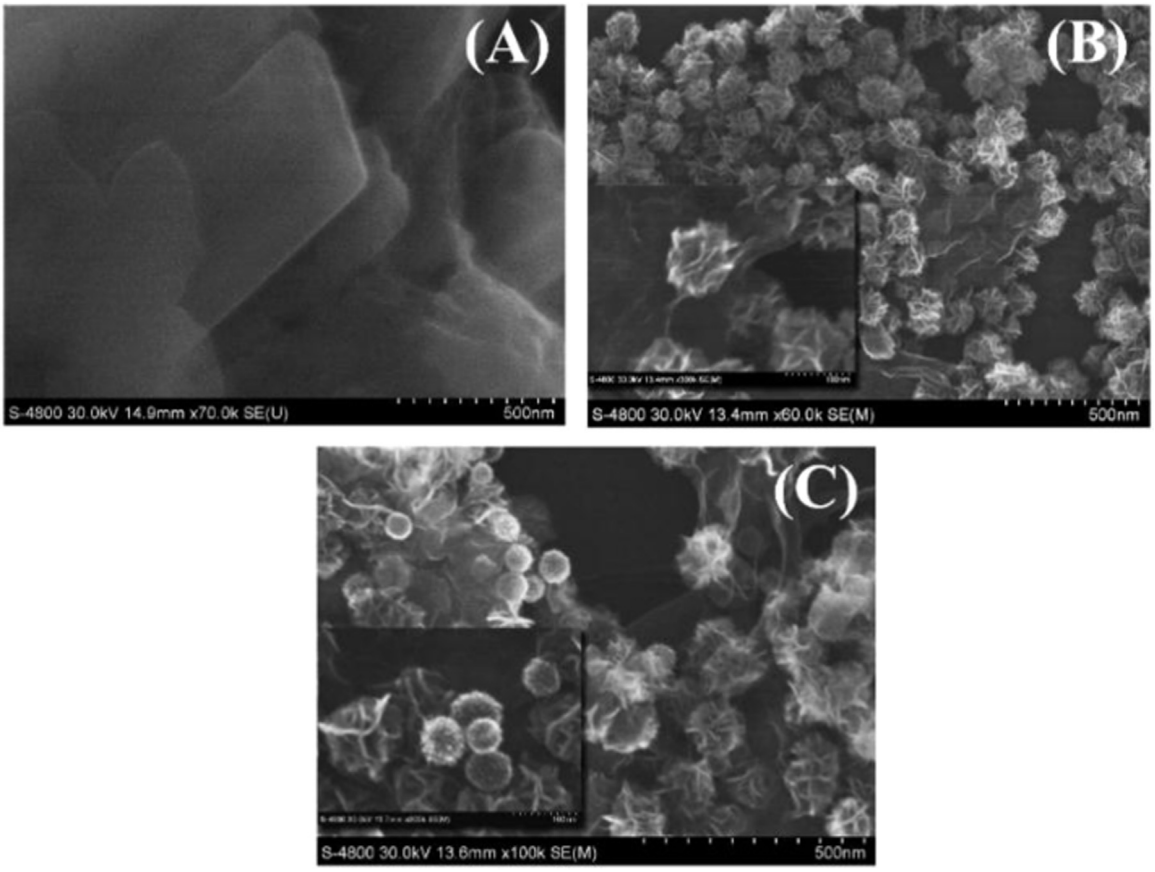

Fig. 1. SEM images of (A) hemin@rGO, (B) fMnO_2-hemin@rGO and (C) hAuPd-fMnO_2-hemin@rGO.

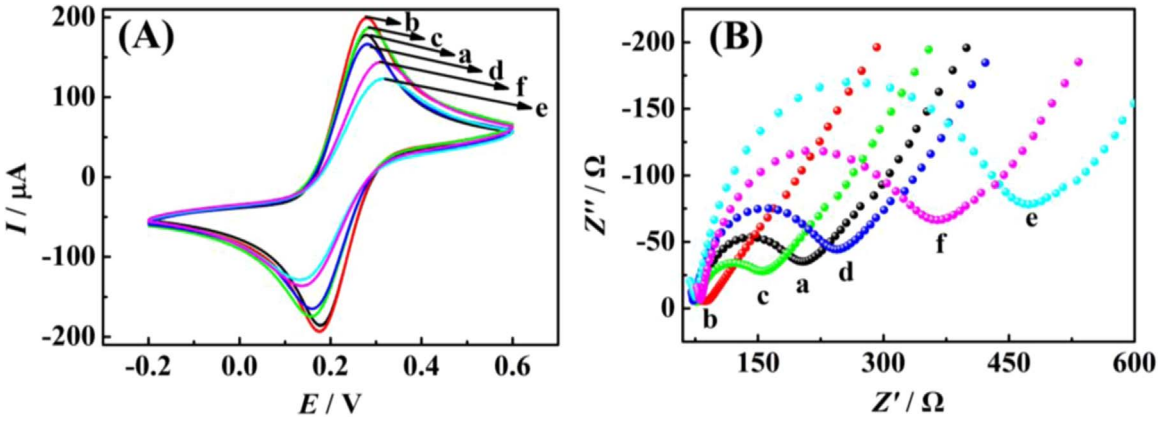

Fig. 2. (A) CV and (B) EIS characterization of different modified electrode in 5 mM $[Fe(CN)_6]^{3-/4-}$ solution (pH 7.4): (a) GCE, (b) depAu/GCE, (c) S1/depAu/GCE, (d) S2/S1/depAu/GCE, (e) BSA /S2/S1/depAu/GCE, and (f) Pb^{2+}/BSA /S2/S1/depAu/GCE.

hybridization reaction of S1 and S2, the decreased peak currents of the electrodes of S1/depAu/GCE and S2/S1/depAu/GCE were obviously observed (curve c and d). This was originated from the hindering of S1 and the formed Pb^{2+}-dependent DNAzyme to electron transfer. The subsequent incubation of the non-conductive BSA as the blocking agent produced again the decreased peak current (electrode BSA/ S2/S1/depAu/GCE, curve e). The final introduction of 100 nM Pb^{2+} standard solution on the electrode BSA/S2/S1/depAu/GCE led to the retrieve of the response signal (electrode Pb^{2+}/BSA/S2/S1/depAu/GCE, curve f), owing to the fact that, in the presence of Pb^{2+}, S1 in the DNAzyme was specifically identified and cleaved by Pb^{2+} into two fragments at rA. The dissociation of one fragment of S1 and S2 from the specific DNAzyme and further leakage from the electrode surface reduced the obstacle of DNAzyme to electron transfer.

Furthermore, electrochemical impedance spectroscopy (EIS) were also measured to characterize the fabrication of the electrochemical sensor. In Fig. 2(B), compared with bare GCE (curve a), the introduction of depAu on the electrode surface resulted in an obvious decrease of the electron transfer impedance (curve b), which indicated the improvement of AuNPs to the electron transfer. Upon the immobilization of S1 and S2 onto the electrode depAu/GCE, the semicircle diameter increased obviously (curve c and d), suggesting the hindrance of S1 and the specific DNAzyme formed by the hybridization of S1 and S2 to the electron transfer. Additionally, the incubation of BSA with inert property to block

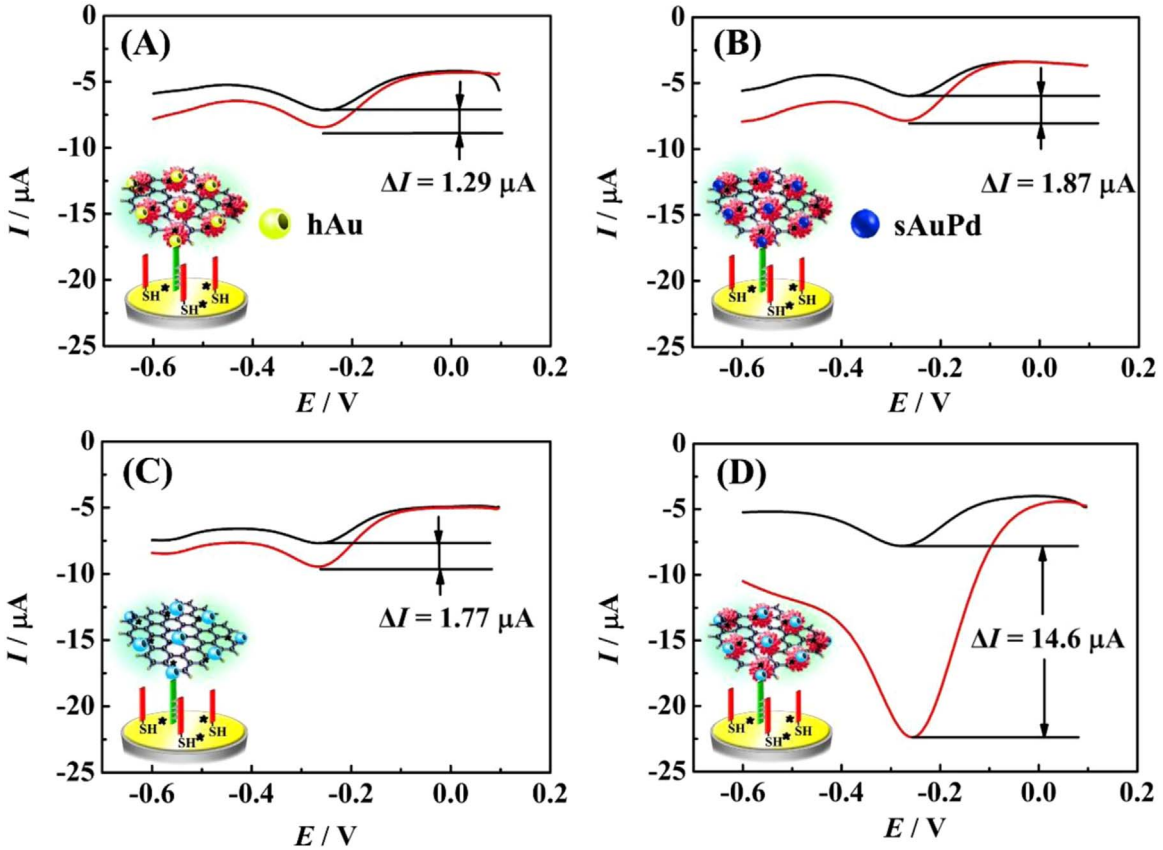

Fig. 3. DPV responses of the electrochemical sensor incubated with 2.5 μM Pb^{2+}-dependent DNAzyme, and 100 nM Pb^{2+} using different bioconjugates: (A) S3-hAu-fMnO_2-hemin@rGO, (B) S3-sAuPd-fMnO_2-hemin@rGO, (C) S3-hAuPd-hemin@rGO and (D) S3-hAuPd- fMnO_2-hemin@rGO measured in 0.1 M PBS (pH 7.0) before (black line) and after (red line) adding 1.7 mM H_2O_2. (For interpretation of the references to color in this figure legend, the reader is referred to the web version of this article.)

nonspecific sites caused another rising of semicircle diameter (curve e). Finally, the impedance value again decreased (curve f) due to the introduction of 100 nM Pb^{2+} standard solution and the specific cleavage of DNAzyme by Pb^{2+}.

3.3. Comparison of electrochemical sensor with different bioconjugates

Firstly, we optimized the experimental conditions including the concentration of Pb^{2+}-dependent DNAzyme, the incubation time of Pb^{2+}, the volume of H_2O_2 and pH of detection solution (see supporting information). Under the optimal conditions, the electrocatalytic efficiency of the proposed bioconjugates of S3-hAuPd-$fMnO_2$-hemin@rGO as probes was compared with those of other three bioconjugates including S3-hAu-$fMnO_2$-hemin@rGO, S3-sAuPd-$fMnO_2$-hemin@rGO and S3-hAuPd-hemin@rGO. When incubated with 2.5 μM Pb^{2+}-dependent DNAzyme and 100 nM Pb^{2+}, the DPV signal of the sensors with these bioconjugates was measured before and after the addition of 1.7 mM H_2O_2, and the results are shown in Fig. 3. Obviously, the sensor with S3-hAu-$fMnO_2$-hemin@rGO only gave 1.29 μA change of peak current (Fig. 3(A)), while the sensors using S3-sAuPd-$fMnO_2$-hemin@rGO and S3-hAuPd-hemin@rGO exhibited a signal amplification of 1.87 μA and 1.77 μA, respectively (Fig. 3(B) and (C)). However, from Fig. 3(D), a significant increase of 14.6 μA in the DPV peak current was observed for the proposed sensor prepared with the bioconjugates of S3-hAuPd-$fMnO_2$-hemin@rGO after adding 1.7 mM H_2O_2 in PBS. The amplification of response signal resulted from S3-hAuPd-$fMnO_2$-hemin@rGO was almost ten times higher than those of S3-hAu-$fMnO_2$-hemin@rGO, S3-sAuPd-$fMnO_2$-hemin@rGO and S3-hAuPd-hemin@rGO. This suggested that the catalytic ability of hAuPd was more excellent than hAu and sAuPd, and $fMnO_2$ played crucial role for the catalytic amplification in this protocol. By the effective integration of hemin-rGO with hAuPd and $fMnO_2$, the proposed S3-hAuPd-$fMnO_2$-hemin@rGO as probe showed the most significant electrocatalytic efficiency toward H_2O_2 reduction. All the observations may be attributed to the following reasons: (i) hemin-rGO as the loading carrier of nanomaterials possesses good conductivity and large area, which is beneficial for the immobilization of numerous nanomaterials with catalytic activity and biomolecules. Meanwhile, the direct electron transfer of hemin as the redox probe provided the electrochemical sense for Pb^{2+}, and the electrocatalytic ability of hemin as an electrocatalyst also was very favorable for accelerating electron transfer. (ii) The loading of $fMnO_2$ NSs with large specific surface area and electrocatalytic activity in hemin-rGO surface further paved the way for abundant immobilization of hAuPd NPs in $fMnO_2$ NSs. (iii) Under the synergetic electrocatalysis of rGO, $fMnO_2$ and hAuPd to the reduction of H_2O_2, the electron transfer between hemin as the redox probe and the electrocatalysts was greatly facilitated and the electrochemical signal was significantly amplified.

3.4. Analytical performance of the proposed electrochemical sensor

When the proposed sensor was incubated with 2.5 μM Pb^{2+}-

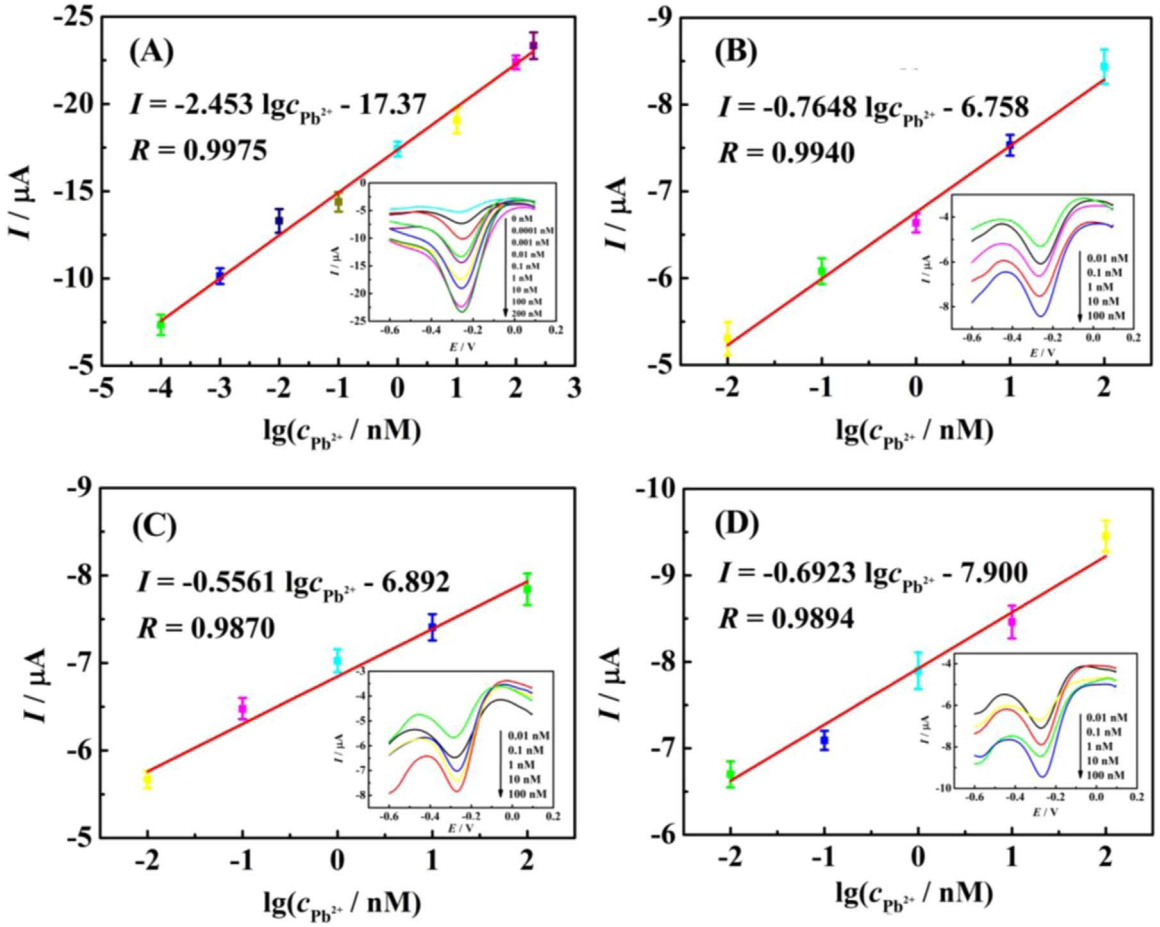

Fig. 4. The calibration plots of the DPV peak current vs. $lgc_{Pb}{}^{2+}$ for the sensor using different bioconjugates: (A) S3-hAuPd-$fMnO_2$-hemin@rGO, (B) S3-hAu-$fMnO_2$-hemin@rGO, (C) S3-sAuPd-$fMnO_2$-hemin@rGO and (D) S3-hAuPd-hemin@rGO. The insets are the DPV responses of the proposed sensors incubated with 2.5 μM DNAzyme and different concentrations of Pb^{2+}, which were measured in 0.1 M PBS (pH 7.0) containing 1.7 mM H_2O_2 under the optimized experiment conditions. Error bars: SD, $n=3$.

dependent DNAzyme and S3-hAuPd-fMnO$_2$-hemin@rGO as probe, the DPV response signal toward different concentrations of Pb^{2+} was investigated. Under the same conditions, the DPV responses of other three sensors were also measured for these bioconjugates including 3-hAu-fMnO$_2$-hemin@rGO, S3-sAuPd-fMnO$_2$-hemin@rGO and S3-hAuPd-hemin@rGO as probes, and the results are shown in Fig. 4. From Fig. 4(A), the DPV response enhanced gradually with the increasing of Pb^{2+} concentration in the range of 0.1 pM–200 nM. The corresponding calibration plots between peak current and the logarithm of Pb^{2+} concentration ($lgc_{Pb}{}^{2+}$) showed a good linear relationship with a regression equation of I (μA) = − 2.453$lgc_{Pb}{}^{2+}$ (nM) − 17.37 and a correlation coefficient of 0.9975. According to the literature (Radi et al., 2006), the limit of detection was defined as LOD = 3s_B/m, where s_B is the standard deviation of the blank and m is the slope of the corresponding calibration curve. Herein, LOD for the proposed sensor was calculated to be 0.034 pM. This could attribute to the fact that the introduction of Pb^{2+} resulted in the specific cleavage of Pb^{2+}-dependent DNAzyme and the immobilization of S3-hAuPd-fMnO$_2$-hemin@rGO bioconjugates through the hybridization reaction between S3 and the cleaved S1 fragment. The more Pb^{2+} was incubated, the more DNAzyme was cleaved, and the more S3-hAuPd-fMnO$_2$-hemin@rGO was captured. So, based on the direct electron transfer of hemin as redox probe, the presence of more hAuPd, fMnO$_2$ and hemin@rGO in the electrode surface cooperatively resulted in the most outstanding electrocatalytic efficiency to H_2O_2 reduction. Meanwhile, from the calibration plots between DPV peak current and $lgc_{Pb}{}^{2+}$ shown in Fig. 4(B)–(D), three sensors with S3-hAu-fMnO$_2$-hemin@rGO, S3-sAuPd-fMnO$_2$-hemin@rGO and S3-hAuPd-hemin@rGO showed lower sensitivity, narrower dynamic linear range and higher LOD, compared with that of S3-hAuPd-fMnO$_2$-hemin@rGO. This further demonstrated that the synergetic electrocatalysis of hAuPd, fMnO$_2$ and hemin@rGO greatly promoted the electron transfer of hemin as the redox probe by accelerating the decomposition of H_2O_2, resulting in the most effective amplification of the electrochemical signal. Based on the specific identification and cleavage of Pb^{2+}-dependent DNAzyme, the proposed Pb^{2+} sensor with S3-hAuPd-fMnO$_2$-hemin@rGO displayed desired analytical performance. The comparison with other methodologies using DNAzyme for detecting Pb^{2+} is shown in Table S2 (see supporting information). Thus, the proposed strategy exhibited more excellent sensitivity, linear range and LOD than these methods based on different signal amplification.

3.5. Specificity, stability and reproducibility of the proposed electrochemical sensor

The specificity of the proposed electrochemical sensor was investigated by measuring DPV response in 0.1 M PBS (pH 7.0) containing 1.7 mM H_2O_2, after respectively incubated with different interfering ions with the same concentration of 1 μM, such as Ba^{2+}, Hg^{2+}, Cd^{2+}, Mg^{2+}, Zn^{2+}, Ca^{2+} and Cu^{2+}, and their mixture with 100 nM Pb^{2+}. As could be seen in Fig. 5, no obvious changes of DPV peak current were observed for the tested interfering ions, whereas the proposed sensor with S3-hAuPd-fMnO$_2$-hemin@rGO exhibited a dramatically increased current signal toward the target Pb^{2+} and its mixture with the interfering irons. Thus, the specificity of the proposed Pb^{2+} sensor was satisfactory.

Additionally, after the proposed electrochemical sensor incubated with 100 nM Pb^{2+} was stored at 4 °C for 10 days, the DPV response was detected in 0.1 M PBS (pH 7.0) containing 1.7 mM H_2O_2. And the observed peak current retained 93.9% of its initial current, indicating a good stability. Under the same experimental conditions, three sensors incubated with 1 nM, 10 nM and 100 nM Pb^{2+} showed almost reproducible DPV response signal. The corresponding relative standard deviations (RSD) of three parallel

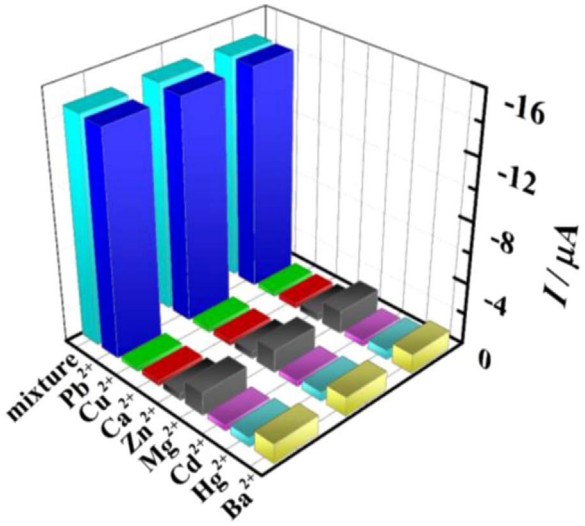

Fig. 5. Specificity of the proposed sensor for 100 nM Pb^{2+} against other metal ions with the same concentration of 1 μM: Ba^{2+}, Hg^{2+}, Cd^{2+}, Mg^{2+}, Zn^{2+}, Ca^{2+}, Cu^{2+} and their mixture with 100 nM Pb^{2+}. Other conditions as shown in figure. Error bars: SD, n = 3.

detections were 4.7%, 7.5%, 3.3%, respectively, suggesting acceptable reproducibility.

3.6. Practical application

To evaluate the applicability of the proposed strategy in actual samples, the developed sensor was used to assay Pb^{2+} in tap water and lake water, which were from the lab and Chongde Lake located in the campus of Southwest University (Chongqing, China). The tap water was used without any treatment and the lake water was treated by centrifuging at 12,000 rpm for 15 min. Firstly, the tap water and lake water were measured by Atomic Absorption Spectroscopy (AAS) method. As a result, the Pb^{2+} content in both tap water and lake water was too low to be detected. Secondly, using the standard addition method, different concentrations of Pb^{2+} with 0.100, 1.00, 10.0 and 100 nM were mixed into the water samples, respectively. After the proposed sensor was incubated with the samples for 60 min, the DPV response was parallelly investigated in 0.1 M PBS (pH 7.0) containing 1.7 mM H_2O_2. The obtained recoveries and RSDs of three determinations are listed in Table S1. As could be seen, the proposed electrochemical sensor showed acceptable recoveries ranging from 99.2% to 107% with 3.19–4.59% of RSD for tap water, and ranging from 98.8% to 108% with 2.96–5.28% of RSD for lake water, respectively. So, the observed experimental results indicated the proposed electrochemical sensor was potentially applicable for detecting Pb^{2+} in real samples.

4. Conclusion

In summary, based on the specific recognition of DNAzyme toward target Pb^{2+}, a novel electrochemical sensor for Pb^{2+} was developed using the nanocomposites of hAuPd-fMnO$_2$-hemin@rGO as electroactive probe and electrocatalysts. The designed probe showed large surface area, high stability, excellent electrocatalytic activity and good redox activity, paving the way for the amplification of electrochemical sensitivity. With the cooperative catalysis of hAuPd, fMnO$_2$ and hemin-rGO toward H_2O_2 reduction, significant amplification of the electrochemical signal was obtained. The proposed Pb^{2+} sensor showed wide linear range, low LOD, good specificity, satisfactory reproducibility and sensitivity.

The proposed strategy may be promising to detect other metal ions by changing the corresponding dependent DNAzyme, making it be potential candidate for highly sensitive electrochemical sensors.

Acknowledgments

We gratefully acknowledge the NNSF of China, China (21275119, 51473136, 21575116) and the Fundamental Research Funds for the Central Universities (XDJK2015A002).

Appendix A. Supporting information

Supplementary data associated with this article can be found in the online version at http://dx.doi.org/10.1016/j.bios.2016.07.111.

References

Chai, J., Li, F.H., Hu, Y.M., Zhang, Q.X., Han, D.X., Niu, L., 2011. J. Mater. Chem. 21, 17922–17929.
Chang, C.R., Long, B., Yang, X.F., Li, J., 2015. J. Phys. Chem. C 119, 16072–16081.
Cui, L., Peng, R.Z., Fu, T., Zhang, X.B., Wu, C.C., 2015a. Anal. Chem. 88, 1850–1855.
Cui, L., Wu, J., Ju, H.X., 2015a. Anal. Chem. 87, 10635–10641.
Cui, L., Wu, J., Ju, H.X., 2015b. Biosens. Bioelectron. 63, 276–286.
Darabdhara, G., Das, M.R., Turcheniuk, V., Turcheniuk, K., Zaitsev, V., Boukherroub, R., Szunerits, S., 2015. J. Mater. Chem. B 3, 8366–8374.
Hou, Y., Cheng, Y.W., Hobson, T., Liu, J., 2010. Nano Lett. 10, 2727–2733.
Jiang, T., Song, Y., Wei, T.X., Li, H., Du, D., Zhu, M.J., Lin, Y.H., 2016. Biosens. Bioelectron. 77, 687–694.
Ju, J., Chen, W., 2015. Anal. Chem. 87, 1903–1910.
Kim, M., Lin, J.W., Kim, H.J., Lee, S.K., Lee, S.J., Kim, T., 2015. Biosens. Bioelectron. 65, 257–264.
Kuo, C.C., Lan, W.J., Chen, C.H., 2014. Nanoscale 6, 334–341.
Li, Q., Wang, Z.L., Li, G.R., Guo, R., Ding, L,X., Tong, Y.X., 2012. Nano Lett. 12, 3803–3807.
Li, S.L., Li, H., Chen, F.J., Liu, J., Zhang, H.L., Yang, Z.Y., Wang, B.D., 2016. Dyes Pigment. 125, 64–71.
Liu, B.Q., Cui, Y.L., Tang, D.P., Yang, H.H., 2012. Chem. Commun. 48, 2624–2626.
Luo, J.H., Li, B.L., Li, N.B., Luo, H.Q., 2013. Sens. Actuators B 186, 83–89.
Radi, A.E., Sanchez, G.L.A., Baldrich, E., O'Sullivan, C.K., 2006. J. Am. Chem. Soc. 128, 117–124.
Shang, L., Zeng, B.Z., Zhao, F.Q., 2015. ACS Appl. Mater. Interfaces 7, 122–128.
Wan, L., Wang, P.J., Su, Y., Wang, L.H., Pan, D., Aldalbahi, A., Yang, S.L., Zuo, X.L., 2015. ACS Appl. Mater. Interfaces 7, 25618–25623.
Wang, H.W., Lang, Q.L., Li, L., Liang, B., Tang, X.J., Kong, L.G., 2013. Anal. Chem. 85, 6107–6112.
Wang, M.H., Zhang, S.A., Ye, Z.H., Peng, D.L., He, L.H., Yan, F.F., Yang, Y.Q., Wu, P.W., Hwang, K., Lan, T., Lu, Y., 2013. J. Am. Chem. Soc. 135, 5254–5257.
Xiao, Y., Rowe, A.A., Plaxco, K.W., 2007. J. Am. Chem. Soc. 129, 262–263.
Zang, Y., Lei, J.P., Hao, Q., Ju, H.X., 2014. ACS Appl. Mater. Interfaces 6, 15991–15997.
Zhang, B., Liu, J., Ma, X.R., Zuo, P., Ye, B.C., Li, Y.C., 2015. Biosens. Bioelectron. 80, 491–496.
Zhang, J., Tang, Y., Teng, L.M., Lu, M.H., Tang, D.P., 2015. Biosens. Bioelectron. 68, 232–238.
Zhang, X.L., Zheng, C., Guo, S.S., Li, J., Yang, H.H., Chen, G.N., 2014. Anal. Chem. 86, 3426–3434.
Zhang, Y., Su, M., Ge, L., Ge, S.G., Yu, J.H., Song, X.R., 2013. Carbon 57, 22–23.
Zhang, Z.X., Balogh, D., Wang, F., Willner, I., 2013. J. Am. Chem. Soc. 135, 1934–1940.
Zhou, Q., Lin, Y.X., Lin, Y.P., Wei, Q.H., Chen, G.N., Tang, D.P., 2015. Biosens. Bioelectron. 78, 236–243.